### Title
The behavior of lipid debris left on cell surfaces from microbubble based ultrasound molecular imaging




### Journal
Ultrasonics, 54(8)

### ISSN
0041-624X



### Authors
Ibsen, Stuart
Shi, Guixin
Schutt, Carolyn
et al.



### Publication Date
2014-12-01

### DOI
10.1016/j.ultras.2014.06.020

Peer reviewed

Published in final edited form as:
*Ultrasonics*. 2014 December ; 54(8): 2090–2098. doi:10.1016/j.ultras.2014.06.020.

# The Behavior of Lipid Debris Left on Cell Surfaces from Microbubble Based Ultrasound Molecular Imaging

**Stuart Ibsen**[1,*], **Guixin Shi**[2], **Carolyn Schutt**[1], **Linda Shi**[1], **Kyle-David Suico**[1], **Michael Benchimol**[2], **Viviana Serra**[1], **Dmitri Simberg**[2], **Michael Berns**[1], and **Sadik Esener**[3]

Stuart Ibsen: sibsen@ucsd.edu

[1]Department of Bioengineering, Moores Cancer Center, University of California San Diego, 3855 Health Sciences Dr. # 0815, La Jolla, CA 92093-0815, Phone (858) 534-9848, Fax: (858) 534-9830

[2]Moores Cancer Center, University of California San Diego, La Jolla, CA 92093 USA

[3]Department of Nanoengineering, Moores Cancer Center, University of California at San Diego, La Jolla, CA 92093 USA

## Abstract

Lipid monolayer coated microbubbles are currently being developed to identify vascular regions that express certain surface proteins as part of the new technique of ultrasound molecular imaging. The microbubbles are functionalized with targeting ligands which bind to the desired cells holding the microbubbles in place as the remaining unbound microbubbles are eliminated from circulation. Subsequent scanning with ultrasound can detect the highly reflectant microbubbles that are left behind. The ultrasound scanning and detection process results in the destruction of the microbubble, creating lipid fragments from the monolayer. Here we demonstrate that microbubbles targeted to 4T1 murine breast cancer cells and human umbilical cord endothelial cells leave behind adhered fragments of the lipid monolayer after exposure to ultrasound with peak negative pressures of 0.18 and 0.8 MPa. Most of the observed fragments were large enough to be resistant to receptor mediated endocytosis. The fragments were not observed to incorporate into the lipid membrane of the cell over a period of 96 min. They were not observed to break into smaller pieces or significantly change shape but they were observed to undergo translation and rotation across the cell surface as the cells migrated over the substrate. These large fragments will apparently remain on the surface of the targeted cells for significant periods of time and need to be considered for their potential effects on blood flow through the microcapillaries and potential for immune system recognition.



*Corresponding Author.

**Keywords**

Lipid Debris; Microbubble; Ultrasound Molecular Imaging; Microbubble Targeting

## 1. Introduction

Microbubbles are extremely reflective to ultrasound pressure waves due to the density difference between the gas and the surrounding water. [1] This reflectivity allows them to function as effective ultrasound contrast agents [2, 3] where they significantly increase the reflectance of the veins and arteries they flow through. [4, 5] This creates a high degree of contrast with the surrounding tissue as detected by standard ultrasound imaging scanners. The absence of microbubbles from a region of normally vascularized tissue is an indication of occlusions or other circulation abnormalities. [5]

The strategy of ultrasound molecular imaging is to use the presence of microbubbles rather than their absence as a diagnostic. The microbubbles are modified on the surface to carry targeting ligands which bind to specific cell surface proteins allowing the microbubbles to accumulate in tissue where the endothelial cells express the protein. [6] An example of a surface protein used for cancer detection is αvβ3 integrin which is expressed on endothelial cells in neovasculature. [7] Expanding tumors require an expanding blood supply in order to provide necessary oxygen and nutrients. [8-10]. The microbubbles that stick to the αvβ3 integrin can remain in the tissue while the other free unbound microbubbles are eliminated from circulation within a few minutes after injection.[11] These remaining microbubbles can then be detected by scanning the tissue region with ultrasound looking for their reflections to reveal the location of the neovasculature. [6, 12] The detection of adhered microbubbles in a suspected tumor lesion can reveal the existence of neovasculature to help increase the accuracy of cancer diagnosis.

The targeting ligands are attached to the lipid monolayer that surrounds the surface of the microbubble and stabilizes the microbubble's gas filled core. [13, 14] These lipid monolayers extend the circulation half-life of the microbubbles significantly allowing them to be viable imaging contrast agents. The gas core of the microbubble is a perfluorocarbon gas and air mixture designed to keep the microbubble at a stable size while in circulation. [15, 16] Incorporating a small fraction of lipids attached to a polyethylene glycol (PEG) polymer chain in the 2000 to 5000 molecular weight size range helps prevent the microbubbles from coalescing in storage and helps protect them during circulation. A fraction of these PEG chains are modified to allow covalent binding to the targeting ligands so they can be accessible above the PEG brush layer. Here two targeting ligand types were studied. The first was the anti-EpCAM antibody which binds to EpCAM expressed on the surface of 4T1 murine breast cancer cells [17]. The second ligand type was the short cyclic RGD peptide which binds to αvβ3 integrin expressed on the surface of endothelial cells in neovasculature [18, 19].

The microbubbles are eventually destroyed by the ultrasound pulses that are used to image them. The microbubbles oscillate with the compression and rarefaction phases of the ultrasound wave. During this process the microbubbles shed lipid fragments [20] and lose a

portion of their gas content with each expansion and contraction cycle until the whole microbubble shrinks to the collapse radius. [21] Under the right conditions and when the ultrasound peak negative pressure is high, the microbubbles can undergo inertial cavitation, producing a shockwave that ruptures the lipid layer. [22]

To understand how these lipid monolayer fragments interact with cell surfaces, we used fluorescence imaging to track labeled lipid fragments generated by microbubble exposure to ultrasound. Understanding the fate of these lipid debris particles is critical to understanding the side effects that could result from the debris of the microbubble itself. Larger particles that remain in the capillaries could create restriction and obstruction points in the microcapillaries changing the normal flow of red blood cells. [23] This could affect tissues that already have a low level of perfusion. The presence of the lipid particles could also stimulate an immune response [24, 25].

## 2. Materials and Methods

Perfluorohexane was purchased from Sigma-Aldrich (St. Louis, MO, USA). Distearoyl phosphatidylcholine (DSPC), was purchased from Avanti Polar Lipids, Inc. (Alabaster, AL, USA). 2-distearoyl-sn-glycero-3-phospho-ethanolamine-N-[maleimide (polyethylene glycol)-3400] (DSPE-PEG3400-Malemide) was purchased from Laysan Bio, Inc. (Arab, AL, USA). DiO was purchased from Biotium, Inc. (Hayward, CA, USA). The trypsin (.25% T / 2.21 mM EDTA) was purchased from Mediatech Inc. (Manassas, VA, USA). Human Umbilical Vein Endothelial Cells (HUVEC) and 4T1 breast carcinoma cells were purchased from the American Type Culture Collection (ATCC) (Manassas, VA, USA). EBM-2 media was purchased from Lonza Inc (Basel, Switzerland). The cRGD was purchased from Anaspec Incorporated (Fremont, CA, USA). The penicillin-streptomycin used in the EBM-2 media was purchased from Gibco (Invitrogen, Grand Island, NY, USA). The fetal bovine serum used in the EBM-2 media solution was purchased from Hyclone (Logan, UT, USA). The PBS was purchased from Hyclone Laboratories Inc. (Logan, UT, USA). All water was purified using the Milli-Q Plus System (Millipore Corporation, Bedford, USA). Purified rat anti-mouse CD326 antibody was obtained from Bio Legend (San Diego, CA, USA).

### 2.1. Cell Culture

The human umbilical vein endothelial cells (HUVEC) were cultured under standard conditions using EBM-2 media with pen/strep from Hyclone and 10% FBS from Invitrogen as well as the ATCC® Endothelial Cell Growth Kit-VEGF. At around 80% confluency the adherent cells were passaged using Trypsin (.25% T / 2.21 mM EDTA) to detach them from the expansion flask and were reseeded into new expansion flasks.

The 4T1 cells were cultured in RPMI 1640 supplemented with 10% heat-inactivated FBS and 100 mg/ml pen/strep using standard techniques.

Both types of cells were incubated at 37°C in a humidified incubator with an atmosphere that contained 5% $CO_2$.

### 2.2. Microbubble Preparation

Microbubbles were prepared using probe sonication techniques that formed both the microbubbles themselves and simultaneously coated them with the stabilizing lipid monolayer. The lipid monolayer was composed of 1,2-distearoyl-sn-glycero-3-phosphocholine (DSPC), PEG 40 stearate, and 2-distearoyl-sn-glycero-3-phospho-ethanolamine-N-[maleimide (polyethylene glycol)-3400] (DSPE-PEG3400-Malemide). All three components were dissolved in chloroform and added together into a 2ml glass vial in a molar ratio of 10:1:1 creating a total lipid content of 100 nanomoles. To fluorescently label the microbubbles, 5 μL of 1 mM DiO in chloroform was also added. The chloroform was evaporated from the solution under an argon stream leaving a lipid film. The film was rehydrated by adding 1ml of PBS and then vortexing vigorously for 30 seconds. The headspace of the vial was filled with an air and perfluorohexane (PFH) gas mixture. Obtaining the correct ratio between air and PFH was critical in preventing the microbubbles from undergoing any osmotically-driven size changes. This stable gas ratio was obtained by filling a 5 ml syringe with 0.5 ml of liquid PFH liquid and rotating it to allow the PFH to coat the sides of the barrel. It was then allowed to sit for 3 min to allow the PFH to evaporate and establish equilibrium with the 4.5 ml of air inside the syringe. This created a mixture that was naturally stable at atmospheric pressure and temperature. A microbubble filled with pure air would quickly dissolve away into the water and collapse. Using a concentration of PFH gas that was too high would result in the PFH condensing into a liquid droplet collapsing the microbubble. A concentration of PFH that was too small would create an osmotic driving force that forced the nitrogen out reducing the microbubble to its collapse radius [15, 16].

The PFH/air mixture was then injected into a glass vial containing the lipid water mixture and was sealed with a parafilm barrier over the top. Care was taken to not inject any liquid PFH by bending the syringe needle at a 130° angle to keep the liquid at the bottom of the syringe near the plunger [26]. The pure air that was originally in the head space of the vial was forced out through the needle track made in the parafilm as 4 ml of the PFH/air mixture was injected in.

The microbubbles were then created by probe sonication at the liquid/gas interface in short 3 second pulses using a Fisher Scientific Model 100 Sonic Membrane Disruptor at a power of 25 W. The microbubble sample was washed 3 times to remove excess phospholipid fragments and deflated microbubbles. The washes consisted of centrifugation at 1500 rpm for 30 seconds and replacement of the PBS. Most of the microbubbles resulting from this process ranged in diameter from 2 – 10 μm.

### 2.3. Microbubble Functionalization with Anti-EpCAM Antibodies

Anti-EpCAM antibodies were attached to the surface of these pre-made microbubbles using anti-Fc fragment specific IgG as a linker. The technique was developed by Shi et al. [17] to target 4T1 cancer cells and is briefly described here. Anti-Fc fragment specific IgG had reactive sulfhydryl groups created on them through reaction with Traut's reagent. A Zeba Spin Desalting Column was use to purify the anti-Fc IgG from the excess Traut's reagent. Once purified, these thiolated IgG's were incubated with the microbubbles to react with the

surface maleimides at room temperature under constant agitation for 1 hour. These anti-Fc IgG functionalized microbubbles were washed three times by centrifugation to remove the excess anti-Fc IgG. These functionalized microbubbles were subsequently incubated with the anti-EpCAM antibodies to allow the Fc region to bind to the anti-Fc IgG. This functionalized the surface of the microbubble with the anti-EpCAM antibodies. The microbubbles were stored at 4°C. 5 μL of 1 mM DiO in chloroform was added to these liposomes for fluorescence imaging.

### 2.4. Microbubble Functionalization with Cyclic RGD Peptide

To target the αvβ3 integrin expressed on the surface of the HUVECs the microbubbles were encapsulated within cRGD functionalized liposomes as described in Ibsen et al.[26] The outer liposomes were functionalized with cRGD by first binding the cRGD to DSPE-PEG (MW = 3400) by adding cRGD dissolved in methanol drop wise to an equal volume of DSPE-PEG-maleimide (MW = 3400) dissolved in chloroform creating a 1:1 molar ratio. This mixture was stirred for 2 hours at room temperature. Chloroform was added to adjust the final volume to achieve a 4mM concentration. 16 μL of the 4mM cRGD lipid construct was added to constitute 40% of the final PEGylated lipid content in the liposome. 5 μL of 1 mM DiO in chloroform was added to these liposomes for fluorescence imaging.

### 2.5. Rose Chamber Preparation

Rose Chambers were used to hold the cells during ultrasound ensonation. The chambers securely contain a media sample between two glass cover slips separated by a rubber gasket as shown in Figure 1. The two glass cover slips and intervening gasket were held in compression by two external aluminum plates. This created a 4ml sized gap that the cell culture media could be injected into allowing the cells to be in a controlled environment for a period of 24 hours. It also allowed the cells to be surrounded by cell culture media while being partially submerged in the water tank used to couple the ultrasound energy from the transducer to the cells themselves. The glass cover slips were 0.13mm thick which was thin enough to allow ultrasound to propagate from the transducer through the water tank and into the Rose Chamber cell culture media with very little attenuation.

Cells were detached from the expansion flask with a 2 min trypsin (.25% T / 2.21 mM EDTA) incubation and suspended in 4ml of cell culture media. The cells were counted and diluted so that 10,000 cells were then injected into a Rose Chamber [27] These low densities made sure the cells would be spatially isolated from one another so the ultrasound/ microbubble interaction events would affect only single cells or small clusters of cells. The media was then injected into Rose Chambers being careful not to introduce air bubbles. The cells were allowed to settle and attach to the glass cover slip overnight before use.

### 2.6. Ultrasound and Microscopy Instrumentation

The cells in the rose chamber were exposed to ultrasound using a custom built system that is shown in Figure 2. A full description of the system is given in Ibsen et al. 2012 [28] and is briefly described here. A water tank was used to acoustical couple the transducer and the Rose Chamber. Ultrasound pulses were generated using a submersible 2.25 MHz transducer (V305-Su 1” spherical-focus, Panametrics, Waltham, MA, USA) with a waterproof

connector cable (BCU -58 - 6W, Panametrics, Waltham, MA, USA). An arbitrary waveform generator (PCI 5412, National Instruments, Austin, TX, USA) was controlled by a custom automation program (LabVIEW 8.2, National Instruments, Austin, TX, USA) to produce the desired waveforms. A 300 W amplifier (VTC2057574, Vox Technologies, Richardson, TX, USA) was used to drive the transducer creating peak negative pressures at the focal region of up to 0.8 MPa. A needle hydrophone (HNP-0400 Broadband Needle Hydrophone AH - 2020-100 with hydrophone pre amp, 50kHz - 100 MHz, 0 +20 dB, Onda Corporation, Sunnyvale, CA, USA) was used to measure the sound field. The short term interactions between the microbubbles and the cells were documented using a high speed camera (FASTCAM 1024 PCI, Photron, San Diego, CA, USA).

The Rose Chamber containing the cells was placed at the air-water interface so that a 100X oil immersion objective (Nikon, Melville, NY, USA) could be used for fluorescent imaging as shown in Figure 2. The Rose Chamber was flipped from its orientation during the over night cell incubation so that the cells were up at the top of the rose chamber to be within the short working distance of the microscope objective. The ultrasound transducer was aligned to focus at the top of the Rose Chamber at the level of the cells. The cover slip region over the cells was not in contact with air due to the oil that optically coupled the objective to the cover slip. The oil prevented the cover slip from becoming a significant reflective surface to the ultrasound. The 0.13mm thick bottom cover slip of the Rose Chamber was thin enough to have little affect on the ultrasound as it focused through it. Sufficient focused energy reached the surface of the Rose Chamber to cause ultrasound/microbubble interaction without causing visible disturbance to non-echogenic liposome membranes [26] or cell membranes. The attenuation of the ultrasound due to the cover slip was below the detection limit of the needle hydrophone.

Once in place, the Rose Chamber was visually scanned using the microscope optics to identify cells that had fluorescent microbubbles attached to the surface. The identified cells were aligned with the ultrasound transducer and were ensonified with a single 2.25 MHz, 10ms, 0.8 MPa peak negative pressure sine wave pulse.

### 2.7. Longitudinal Observations of Cell Surfaces

The longitudinal observations of the live cells in the Rose Chambers were made using a Zeiss Axiovert 200M Microscope (Zeiss, Thornwood, NY) with a 63× phase III, NA 1.4 oil immersion objective. A Green Fluorescent Protein filter cube from Chroma (Rockingham, VT, USA) was used for the fluorescent images. All microscope control and imaging utilized the RoboLase II system. [29] This microscope system was used because it could take both phase contrast and fluorescent images of the cells allowing both images to be merged together. It also had a heated stage to keep the cells at 37°C for extended periods of time allowing observations of the cell surfaces to be made over longer time periods.

### 2.8 Ultrasound Pulse Characteristics

The cells were exposed to a single 2.25 MHz ultrasound pulse that was 10 ms in duration. The compression and rarefaction phases of the ultrasound wave have been shown to shrink and expand the microbubbles to half and 4 times their original diameter.[21, 30-32]

Two different peak negative pressures were used. The first was 0.18 MPa to study how the microbubbles would respond to conditions where the microbubbles would not produce shockwaves. Inertial cavitation of microbubbles has been shown to occur with peak ultrasound pressures above 0.6 MPa.[33]. The second peak negative pressure used was 0.8 MPa.

The ultrasound waves propagated through pure cell culture media and distilled water in containers that were significantly larger than the wavelength of the ultrasound. The glass cover slip that the ultrasound passed through to reach the cells was 0.13mm thick and the cells were arranged in monolayers. All these factors should prevent nonlinear behavior in the acoustic wave.

### 2.9. Experimental Procedure

Cells were cultured and seeded into Rose Chambers as described above and incubated at 37°C overnight to allow them to adhere to the glass cover slip of the Rose Chamber. 10 μl of the fluorescent DiO labeled ligand functionalized microbubbles were injected into the Rose Chamber and the chamber inverted so the cells were at the top. This allowed the diluted microbubble sample to float to the top of the chamber and bind to the adherent cells. After 10 min of incubation the chamber was tilted at a 45° angle to allow the non-adhered microbubbles to float up to the corner and out of the way. The Rose Chamber was then returned to a horizontal position for ultrasound exposure.

The chamber was placed into the ultrasound/microscope setup. The chamber was scanned to find a cell which had adherent microbubbles. The cell was centered in the ultrasound focal zone. The microbubble interaction with the ultrasound and the cell was documented using the high speed fluorescent videography capabilities of the system. All of these actions were conducted at room temperature.

To follow the lipid particles on the surface of the cells for a longer period of time the Rose Chambers were transferred to the RobolaseII microscope system described in the longitudinal observation section above. The cells could be maintained at 37°C for the entire period of observation. This system allowed both a phase contrast and a fluorescent image to be taken at each time point. The images were merged to produce phase contrast images of the cells with an overlay of the green fluorescent particles using Image J 1.46r Software and Photoshop.

## 3. Results

### 3.1. Lipid Debris Particle Behavior Immediately After Exposure to 0.18 MPa Peak Negative Pressure Ultrasound

The anti-EpCAM functionalized microbubbles were successfully targeted to the surface of the 4T1 cells as shown in Figure 3. These single microbubbles were ensonified with low peak negative pressure ultrasound which caused them to undergo size oscillations resulting in the fragmentation of the lipid monolayer and the dissolution of the gas from the microbubble. Lipid fragments remained attached to the surface of all three cells after ultrasound exposure. These adhered particles were still in place when observed 9 min after

the ultrasound exposure. Free floating particles were observed to move away from the cell surface due to Brownian motion over that time period. The size of these lipid debris fragments were observed to be smaller than the original microbubbles showing that the majority of the lipid monolayer moved away from the surface of the cell. The observed translation of lipid fragments might have been caused by possible fluid microstreaming created by the ultrasound/microbubble interaction [34, 35]

Clusters of microbubbles attached to cell surfaces are shown in Figure 4. When exposed to the low peak negative pressure ultrasound the microbubbles were destroyed and left lipid debris fragments behind on the cell surface. This indicates that if fluid microstreaming flow patterns resulted from the exposure of neighboring microbubbles to the ultrasound [36] it was not strong enough to dislodge the lipid particles from the cell surface. More fragments were left attached to the cell surface per microbubble than that observed for the single microbubbles in Figure 3.

### 3.2. Lipid Debris Particle Behavior Immediately After Exposure to 0.8 MPa Peak Negative Pressure Ultrasound

Lipid debris particles were also left adhered after a HUVEC with a single microbubble was ensonified with high peak negative pressure ultrasound as shown in Figure 5. The interaction between the ultrasound and the microbubble was powerful enough to dislodge the cell from the substrate causing a rotational translation. The image was reregistered to show the same section of the cell in the magnified view. Small lipid debris particles were seen to remain on the surface of the cell despite the intensity of the shockwave and resulting fluid flow. These remaining particles were attached to the cell surface because they stayed in place despite the cell rotation and the observation that other free floating fluorescent particles moved out of the field of view due to the ultrasound/microbubble interaction.

### 3.3. Tracking of the Adhered Lipid Particles

The 4T1 cell populations that were ensonified with low peak negative pressure ultrasound were followed for a period of up to 96 min to determine the behavior of the lipid debris left on the cell surface over time. A single lipid debris particle left behind on the surface of a single 4T1 cell that is part of a small group of non-confluent cells is shown in Figure 6. The particle was shown to undergo rotation and translation on the surface of the cell as the cell moved across the substrate. The particle was not seen to break up or change shape. The lipid particle also did not appear to incorporate into the cell membrane because the DiO lipophilic dye was not shown to spread from the particle to the surrounding cell membrane. It is unlikely that the fragments were endocytosed by the cell because the large fragment sizes of 3 – 6 μm are difficult for these cells to endocytose. [37]

Multiple particles on two different but adjoining 4T1 cells that were not confluent with their neighbors were tracked as shown in Figure 7. Here three particles were shown, the top two are on a single cell and moved closer together over a period of 64 min while the third particle was on a second cell and moved towards the bottom of the field of view. The fluorescence of the two top particles appears to become more diffuse over time and was due to the cell rounding up and raising its surface thereby pushing the particles out of the focal

plane of the objective. Refocusing the image to the same level as the particles showed that the particles were intact and had not incorporated into the cell membrane.

Particles left behind on a single 4T1 cell that was part of a confluent cell monolayer are shown in Figure 8. Like the cells shown in Figures 6 and 7 the particle did not break up, did not appear to be endocytosed and did not incorporate into the cell membrane. The degree of particle translation and rotation was less than what was observed in Figures 6 and 7 probably due to this cell's confluency confinement with the neighboring cells.

The data presented in the figures is summarized in Table 1.

## 4. Discussion

The microbubbles successfully attached to the surface of the 4T1 cells using anti-EpCAM targeting and to the surface of the HUVECs using cRGD targeting. Both types of targeting were strong enough to allow lipid fragments from the microbubble lipid monolayer to remain attached to the surface of the cell after exposure to ultrasound. The fragments that were left behind from exposure to the 0.18 MPa peak negative pressure ultrasound were smaller than the original microbubble and were located at the point of attachment between the microbubble and the cell surface. This indicates that fragments of lipid which were not originally attached to the cell surface did not subsequently attach after the microbubble was destroyed probably due to the ultrasound/microbubble interaction forcing them away from the cell surface. The ultrasound/microbubble interaction may have produced microstreaming which could account for this observation.

Lipid fragments produced from exposure to the 0.18 MPa peak negative pressure ultrasound were larger than the fragments created by exposure to 0.8 MPa peak negative pressure ultrasound indicating that the 0.8 MPa created a more powerful ultrasound/microbubble interaction. The 0.8 MPa peak negative pressure ultrasound could have resulted in the inertial cavitation of the microbubble since inertial cavitation has been documented to occur at peak negative pressures as low as 0.6 MPa. [38] Passive detection methods [39] documented broadband signals produced by the microbubbles when exposed to 0.8 MPa peak negative pressure ultrasound in the experimental setup under these conditions confirming the occurrence of inertial cavitation as described in Schutt et al.[40]. The observed results, with smaller lipid debris particles being produced and the cell being partially detached from the substrate, are consistent with the higher intensity fluid flow and shockwave production caused by inertial cavitation. These indications of intense fluid flow were not seen with any of the microbubbles exposed to 0.18 MPa peak negative pressure ultrasound.

None of the lipid fragments produced appeared to incorporate into the cell membranes they were adhered to. The original lipid monolayers surrounding the microbubbles had a PEG brush layer on the surface which stabilized the microbubbles by creating a barrier which prevented them from merging with one another while in storage. The PEG layer has also been shown to help prolong circulation *in-vivo* by reducing immune recognition. [41, 42] The PEG would have also been present on the lipid fragments and likely prevented the lipid

fragments from coming into physical contact with the cell's lipid membrane thereby hindering their ability to integrate into the cell membrane.

These lipid fragments appear to be stable and can remain attached to the surface of the cells for periods of at least 96 min. A fraction of the particles that were created by microbubble exposure to high peak negative pressure ultrasound would likely be small enough for some to be internalized by receptor mediated endocytosis. The majority of the observed fragments however, would likely be too large for internalization and would remain on the surface of the cell for long periods of time. [43] The larger sized particles could interfere with the blood flow through microcapillaries. The particles could also interact with the immune system since they are essentially tagging the surface of the cell with a foreign body. The PEG layer should hinder the immune recognition of the particles, but the PEG may not cover the surface uniformly leaving gaps that could allow for protein adhesion and immune recognition

## 5. Conclusions

Microbubble targeting using both cRGD to $\alpha v\beta 3$ integrin on HUVECs and anti-EpCAM targeting to EpCAM on 4T1 cells allowed lipid fragments to remain on the surface of the cell after exposure to high and low peak negative pressure ultrasound. These lipid fragments were not seen to incorporate into the cell membrane probably due to the PEG brush layer that was on the surface of the lipid fragments creating a physical barrier to integration. The majority of the lipid particles were too large for receptor mediated endocytosis and so remained on the surface of the cell for at least 96 min. The particles were not seen to break up or significantly change their shape, but they did rotate and translate across the cell surface as the cells migrated across the substrate. The degree of movement was lower in confluent cell monolayers probably due to the confluency restricted motion. Future work will look to understand how these adherent lipid particles may interfere with blood flow through the microcapillaries and how they might interact with the immune system.

## Acknowledgments

The study was supported by Grant Numbers T32 CA121938, R25 CA153915 NCI, and 5U54CA119335-05 from the National Cancer Institute. Support was also provided by the UCSD Cancer Center Specialized Support Grant P30 CA23100 and Department of Defense (Army) IDEA BC095376 to Dmitri Simberg.

## References

1. Mattrey RF. Perfluorooctylbromide: a new contrast agent for CT, sonography, and MR imaging. American Journal of Roentgenology. 1989; 152(2):247–252. [PubMed: 2643258]
2. de Jong N, Bouakaz A, Frinking P. Basic acoustic properties of microbubbles. Echocardiography. 2002; 19(3):229–40. [PubMed: 12022933]
3. Von Bibra H, et al. Interaction of Microbubbles with Ultrasound. Echocardiography. 1999; 16(7, Pt 2):733–741. [PubMed: 11175216]
4. Goldberg BB, Liu JB, Forsberg F. Ultrasound contrast agents: A review. Ultrasound in Medicine & Biology. 1994; 20(2):319–333. [PubMed: 8085289]
5. Cosgrove D. Ultrasound contrast agents: An overview. European Journal of Radiology. 2006; 60(3): 324–330. [PubMed: 16938418]

6. Kaufmann BA, Lindner JR. Molecular imaging with targeted contrast ultrasound. Current Opinion in Biotechnology. 2007; 18(1):11–16. [PubMed: 17241779]
7. Hood JD, et al. Tumor regression by targeted gene delivery to the neovasculature. Science. 2002; 296(5577):2404–2407. [PubMed: 12089446]
8. Mauldin F, et al. Real-time targeted molecular imaging using singular value spectra properties to isolate the adherent microbubble signal. Phys Med Biol. 2012; 57(16):5275–93. [PubMed: 22853933]
9. Couture O, et al. Tumor delivery of ultrasound contrast agents using Shiga toxin B subunit. Mol Imaging. 2011; 10(2):135–43. [PubMed: 21439258]
10. Anderson C, et al. Ultrasound molecular imaging of tumor angiogenesis with an integrin targeted microbubble contrast agent. Invest Radiol. 2011; 46(4):215–24. [PubMed: 21343825]
11. Willmann JK, et al. Targeted microbubbles for imaging tumor angiogenesis: assessment of whole-body biodistribution with dynamic micro-PET in mice. Radiology. 2008; 249(1):212–9. [PubMed: 18695212]
12. Dayton PA, et al. Ultrasonic analysis of peptide-and antibody-targeted microbubble contrast agents for molecular imaging of αvβ3-expressing cells. Molecular imaging. 2004; 3(2):125. [PubMed: 15296677]
13. Borden MA, et al. Surface phase behavior and microstructure of lipid/P EG-emulsifier monolayer-coated microbubbles. Colloids and Surfaces B: Biointerfaces. 2004; 35(3):209–223.
14. Kim DH, et al. Mechanical properties and microstructure of poly crystalline phospholipid monolayer shells: Novel solid microparticles. Langmuir. 2003; 19(20):8455–8466.
15. Schutt E, Pelura T, Hopkins R. Osmotically-stabilized microbubble ultrasound contrast agents. Acad Radiol. 1996; 3:S188–S190. [PubMed: 8796558]
16. Schutt E, et al. Injectable Microbubbles as Contrast Agents for Diagnostic Ultrasound Imaging: The Key Role of Perfluorochemicals. Angew Chem Int Ed. 2003; 42:3218–3235.
17. Shi G, et al. Isolation of Rare Tumor Cells from Blood Cells with Buoyant Immuno-Microbubbles. PloS one. 2013; 8(3):e58017. [PubMed: 23516425]
18. Jin ZH, et al. In vivo optical imaging of integrin Î±. Molecular cancer. 2007; 6:41. [PubMed: 17565663]
19. Yong KT, et al. Synthesis of cRGD-peptide conjugated near-infrared CdTe/ZnSe coreâ€“shell quantum dots for in vivo cancer targeting and imaging. Chem Commun. 2010; 46(38):7136–7138.
20. Borden, MA., et al. Physico-chemical properties of the microbubble lipid shell [ultrasound contrast agents]. Ultrasonics Symposium, 2004 IEEE; 2004;
21. Bloch SH, et al. Optical observation of lipid-and polymer-shelled ultrasound microbubble contrast agents. Applied physics letters. 2004; 84(4):631–633.
22. Kodama T, Tomita Y. Cavitation bubble behavior and bubble–shock wave interaction near a gelatin surface as a study of in vivo bubble dynamics. Appl Phys B. 2000; 70:139–149.
23. Boryczko K, Dzwinel W, Yuen DA. Dynamical clustering of red blood cells in capillary vessels. Journal of molecular modeling. 2003; 9(1):16–33. [PubMed: 12638008]
24. Allison AC, Gregoriadis G. Liposomes as immunological adjuvants. 1974
25. Judge A, et al. Hypersensitivity and loss of disease site targeting caused by antibody responses to PEGylated liposomes. Molecular Therapy. 2006; 13(2):328–337. [PubMed: 16275098]
26. Ibsen S, et al. A novel nested liposome drug delivery vehicle capable of ultrasound triggered release of its payload. Journal of Controlled Release. 2011; 155(3):358–366. [PubMed: 21745505]
27. Rose G. A separable and multipurpose tissue culture chamber. Texas reports on biology and medicine. 1954; 12(4):1074. [PubMed: 13238275]
28. Ibsen S, Benchimol M, Esener S. Fluorescent Microscope System to Monitor Real-Time Interactions between Focused Ultrasound, Echogenic Drug Delivery Vehicles, and Live Cell Membranes. Ultrasonics. 2012 In Press.
29. Botvinick, Elliot; Berns, M. Internet-Based Robotic Laser Scissors and Tweezers Microscopy. Microscopy Research and Technique. 2005; 68:65–74. [PubMed: 16228982]
30. Chin CT, et al. Brandaris 128: A digital 25 million frames per second camera with 128 highly sensitive frames. Review of Scientific Instruments. 2003; 74(12):5026–5034.

31. Chomas JE, et al. Threshold of fragmentation for ultrasonic contrast agents. Journal of biomedical optics. 2001; 6(2):141–150. [PubMed: 11375723]
32. Postema M, et al. High-speed photography during ultrasound illustrates potential therapeutic applications of microbubbles. Medical physics. 2005; 32:3707. [PubMed: 16475770]
33. van der Meer SM, et al. Microbubble spectroscopy of ultrasound contrast agents. The Journal of the Acoustical Society of America. 2007; 121:648. [PubMed: 17297818]
34. Collis J, et al. Cavitation microstreaming and stress fields created by microbubbles. Ultrasonics. 2010; 50(2):273–279. [PubMed: 19896683]
35. Ferrara K, Pollard R, Borden M. Ultrasound Microbubble Contrast Agents: Fundamentals and Application to Gene and Drug Delivery. Annu Rev Biomed Eng. 2007; 9:415–447. [PubMed: 17651012]
36. Tho P, Manasseh R, Ooi A. Cavitation microstreaming patterns in single and multiple bubble systems. J Fluid Mech. 2007; 576:191–233.
37. De S, Miller DW, Robinson DH. Effect of particle size of nanospheres and microspheres on the cellular-association and cytotoxicity of paclitaxel in 4T1 cells. Pharmaceutical research. 2005; 22(5):766–775. [PubMed: 15906172]
38. Miller DL, Thomas RM. Ultrasound Contrast Agents Nucleate Inertial Cavitation In Vitro. Ultrasound in Med & Biol. 1995; 21(8):1059–1065. [PubMed: 8553500]
39. Chen WS, et al. A comparison of the fragmentation thresholds and inertial cavitation doses of different ultrasound contrast agents. The Journal of the Acoustical Society of America. 2003; 113(1):643–651. [PubMed: 12558300]
40. Schutt C. The Influence of Distance Between Microbubbles on the Resulting Shape of Ultrasound-Induced Inertial Cavitation Shockwaves. Under review.
41. Klibanov AL, et al. Amphipathic polyethyleneglycols effectively prolong the circulation time of liposomes. FEBS letters. 1990; 268(1):235–237. [PubMed: 2384160]
42. Moghimi SM. Chemical camouflage of nanospheres with a poorly reactive surface: towards development of stealth and target-specific nanocarriers. Biochimica et Biophysica Acta (BBA)-Molecular Cell Research. 2002; 1590(1):131–139.
43. Wiewrodt R, et al. Size-dependent intracellular immunotargeting of therapeutic cargoes into endothelial cells. Blood. 2002; 99(3):912–922. [PubMed: 11806994]

- Microbubbles successfully attached to the cell surface using targeting ligands
- Ultrasound exposure fragmented the microbubble lipid monolayer
- Lipid fragments from the monolayer remained adhered to the cell surface
- Fragments did not incorporate into the cell lipid membrane over a period of 96 min
- Fragments translated and rotated across the cell surface as the cells migrated

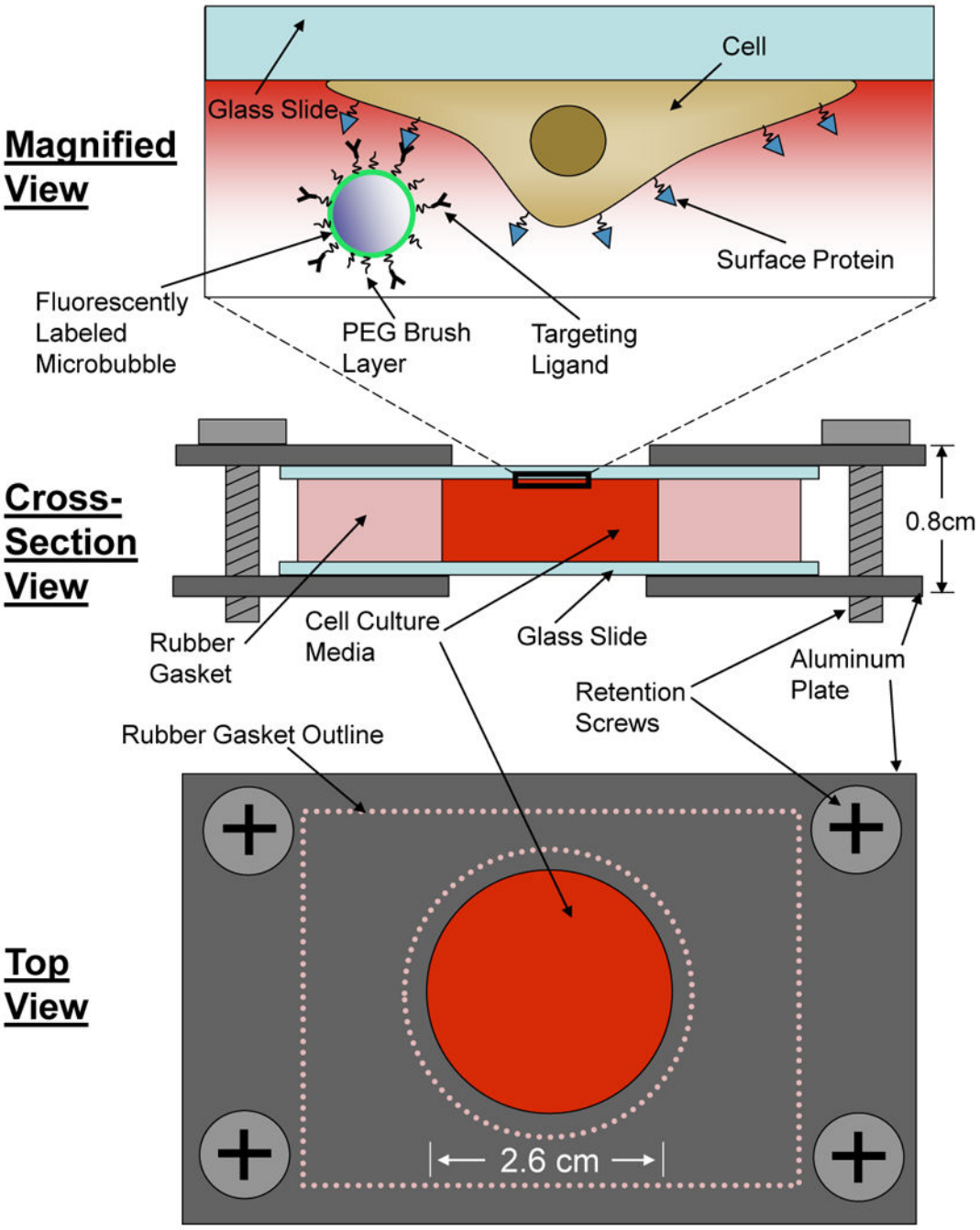


**Figure 1.**

Schematic of the Rose Chamber. The chamber contained 4ml of cell culture media between two glass cover slips held apart by a rubber spacer. The entire structure was held in compression between two aluminum plates. The cells were oriented at the top of the chamber for imaging.

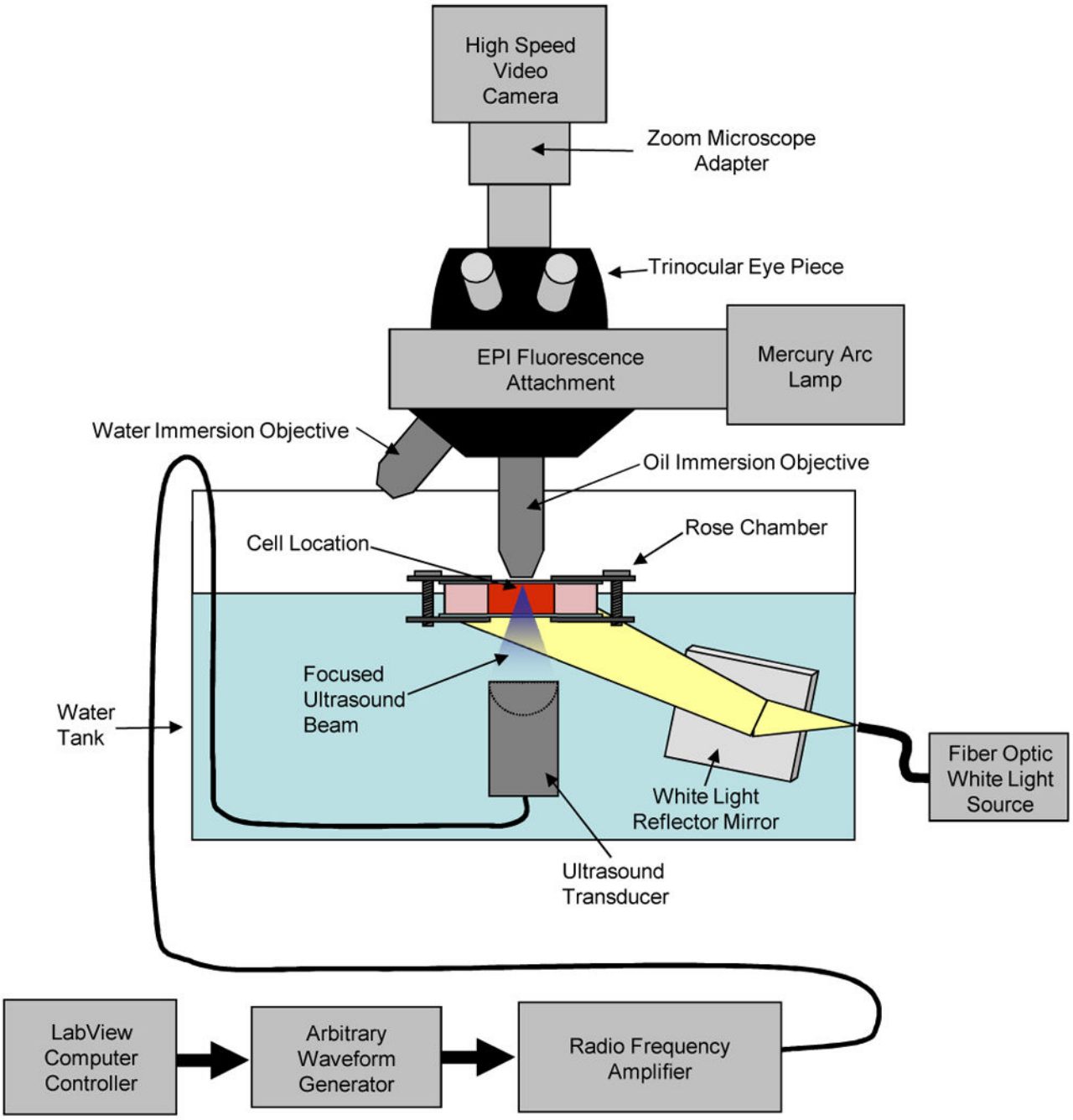


**Figure 2.**

Schematic of the Rose Chamber in the ultrasound ensonation and optical imaging setup. The Rose Chamber containing the cells was partially submerged in the tank of water which coupled the ultrasound from the transducer up to the Rose Chamber. The ultrasound passed, through the bottom cover slip and focused at the level of the cells on the top cover slip. The microbubble interaction with the cells under the influence of ultrasound was observed from above through the 100X oil immersion objective.

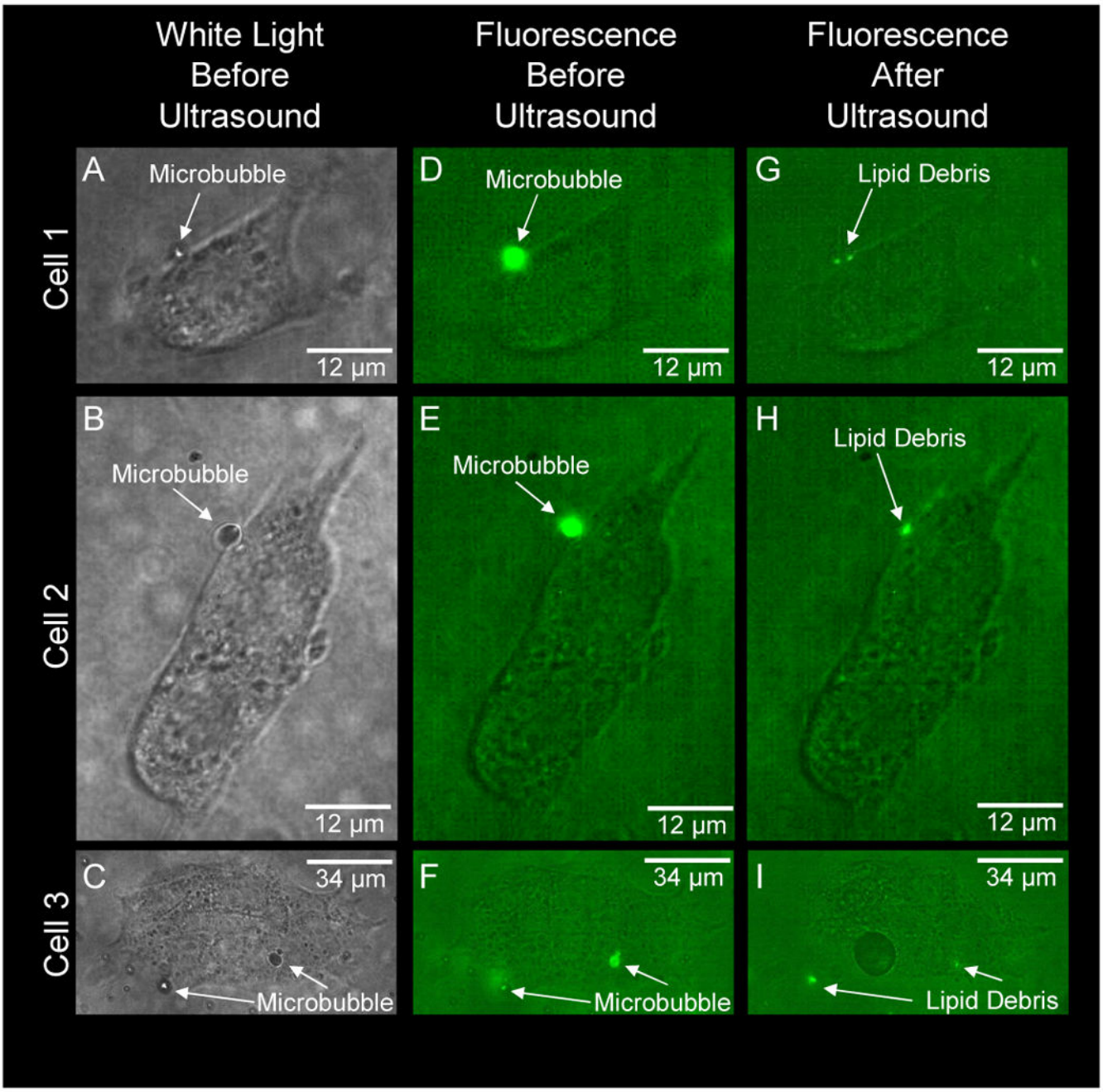


**Figure 3.**

Microbubble lipid monolayer debris left behind on 4T1 murine breast cancer cell surfaces from single isolated microbubbles when exposed to low peak negative pressure ultrasound. Three different cells were exposed to an ultrasound pulse with peak negative pressure of 0.18 MPa. All four microbubbles were 3 μm in diameter. **Panels A, B and C -** The white light image before ultrasound shows the cell with the single microbubble identified by the arrow. **Panels D, E and F -**The fluorescence before ultrasound images show the fluorescently labeled lipid shell of the microbubble also identified by the arrows. **Panels G, H and I -**The fluorescence images after ultrasound exposure show the lipid debris particles

that are left behind on the surface of the cells. These post ultrasound images are taken 17 ms after the ultrasound exposure. Re-imaging the cells after 9 min showed that the identified debris particles were still adhered to the surface of the cell and had not moved away by Brownian motion. Two microbubbles are pointed out on Cell 3. The microbubble on the left is slightly above the focal plane of the objective and the fluorescence appears diffuse in frame F. However in frame I the resulting lipid debris is left in focus.

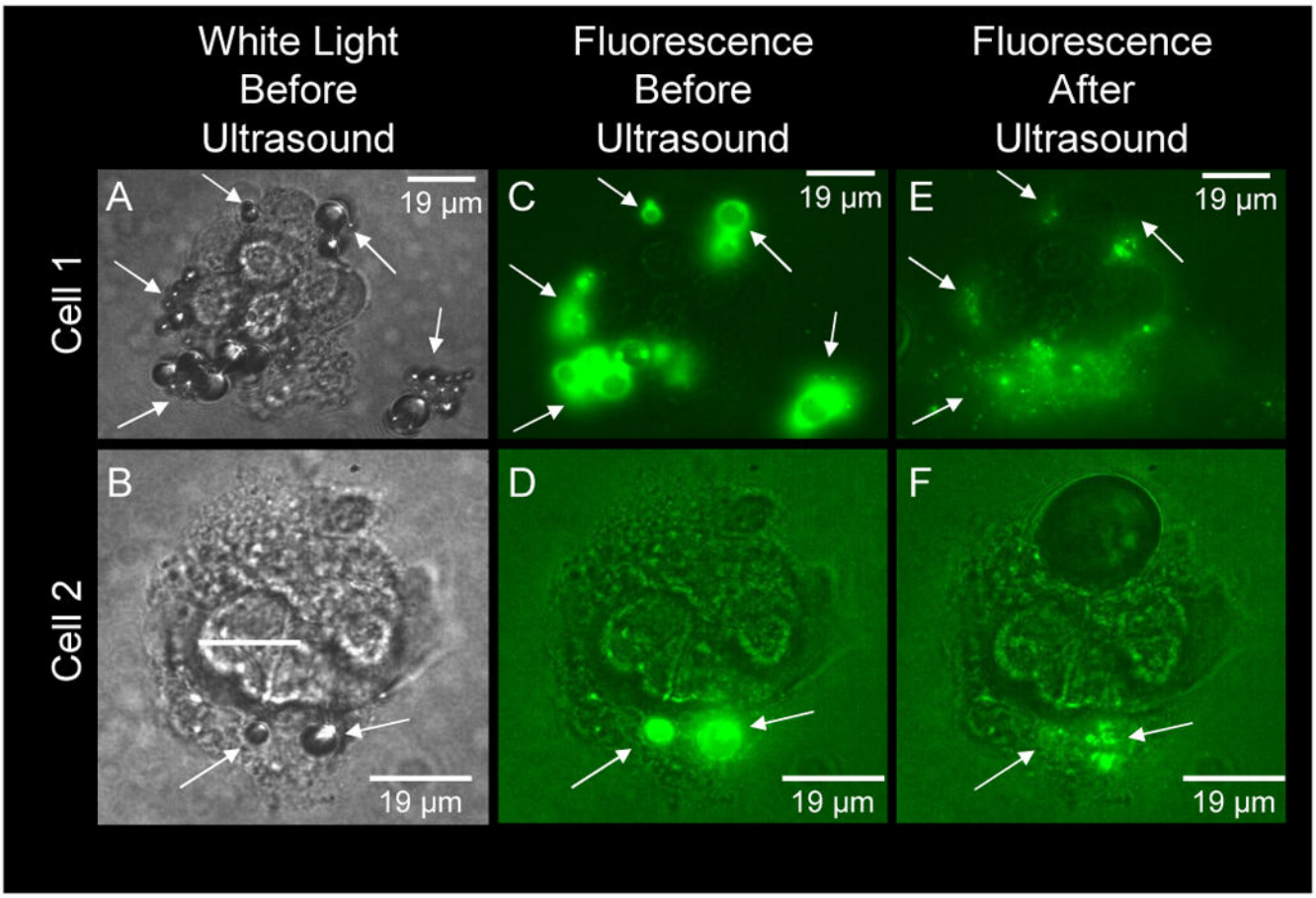


**Figure 4.**

Microbubble lipid monolayer debris left behind on 4T1 murine breast cancer cell surfaces from multiple microbubbles and adjoining microbubble clusters when exposed to low peak negative pressure ultrasound. Two different cells were exposed to an ultrasound pulse with peak negative pressure of 0.18 MPa. **Panels A and B -** The white light image before ultrasound shows the cell with the microbubble clusters identified by the arrows. The cluster of microbubbles in Panel A had sizes that ranged from 2 to 8 μm in diameter. The two microbubbles in Panel B were 5.7 μm and 8.6 μm in diameter. **Panels C and D -** The fluorescence before ultrasound images show the fluorescently labeled lipid shell of the microbubble also identified by the arrows. **Panels E and F -** The fluorescence images after ultrasound exposure show the lipid debris particles that are left behind on the surface of the cells. These after ultrasound images are taken 17ms after the ultrasound exposure. Re-imaging the cells after 9 min showed that the identified debris particles were still adhered to the surface of the cell and had not moved away by Brownian motion. More particles were left attached to the cell per microbubble than for the single microbubbles shown in Figure 3.

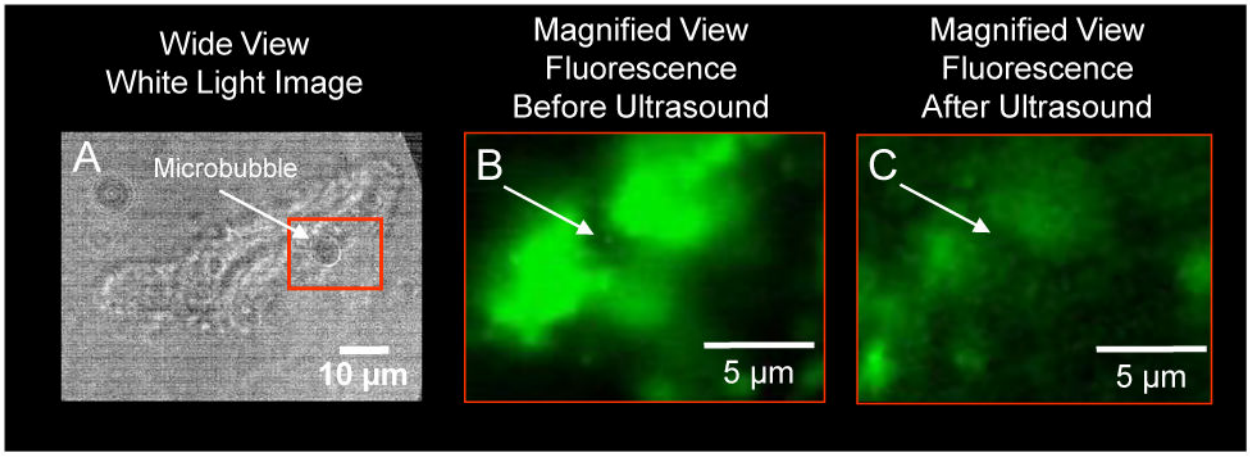


**Figure 5.**

Lipid debris left behind on a HUVEC surface from a single microbubble when exposed to high peak negative pressure ultrasound. Here a single HUVEC has a microbubble adhered to the surface through cRGD targeting to αvβ3 integrin. The field of view was exposed to a single 2.25 MHz ultrasound sine wave with peak negative pressure of 0.8 MPa. The microbubble was 2 μm in diameter. **A** - The white light image before ultrasound shows the cell with the microbubble identified by the arrow. **B** - The fluorescence before ultrasound image shows a magnified view of the boxed region in panel A. Fluorescently labeled lipid particles are seen surrounding the microbubble also identified by the arrow. **C** - The fluorescence image after ultrasound exposure showing the lipid debris particles that are left behind on the surface of the cell. The arrow points to the original microbubble location. These after ultrasound images are taken 17ms after the ultrasound exposure. These particles remained attached to the surface of the cell even though the ultrasound/microbubble interaction was strong enough to partially detach the cell from the substrate.

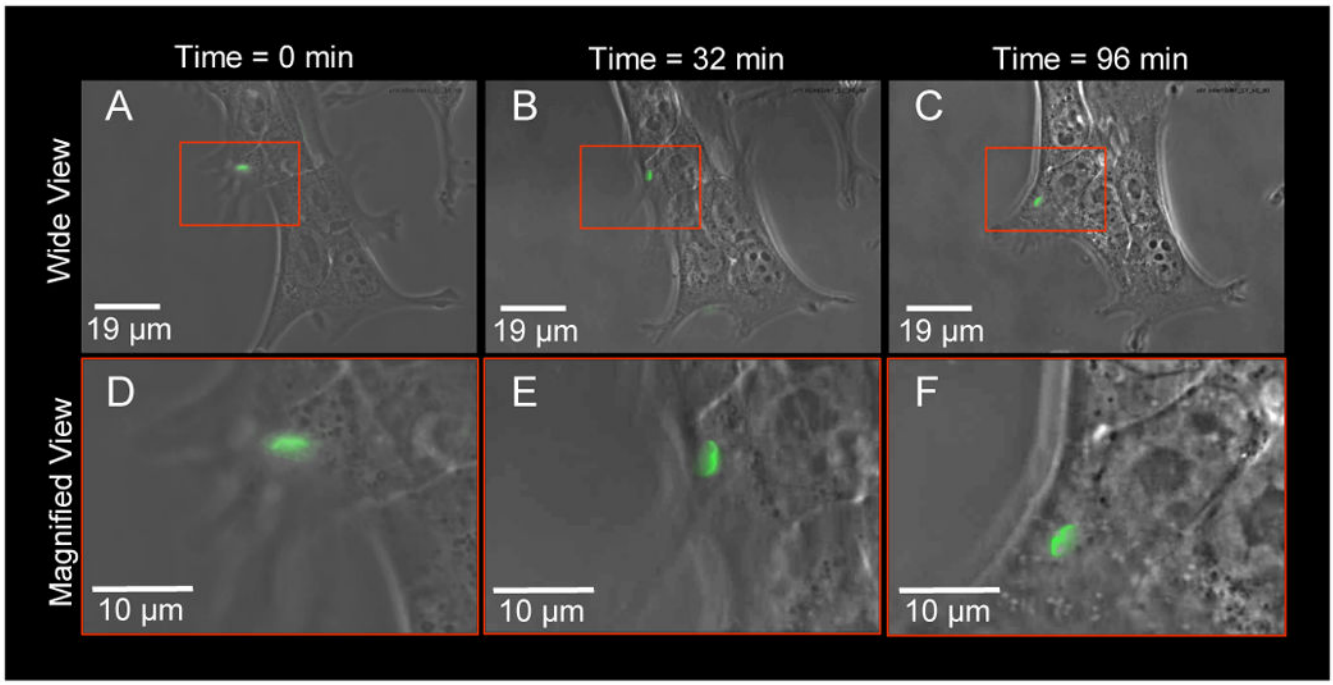


**Figure 6.**

Observation of 1 attached lipid debris particle over time on the surface of a single 4T1 murine breast cancer cell that is part of a small group of cells at three different time points. The particle was left adhered to the cell after low peak negative pressure ultrasound exposure. These are phase contrast images merged with green fluorescent images of the lipid particles. **Panels A, B, and C** show the wide field view of the cell with the lipid fragment shown in green. **Panels D, E, and F** are magnified views of the particles at each time point. The particle did not change shape or appear to integrate into the cell membrane. It did rotate 90° clockwise and then 130° counter-clockwise and translated 11μm as the cell moved across the substrate.

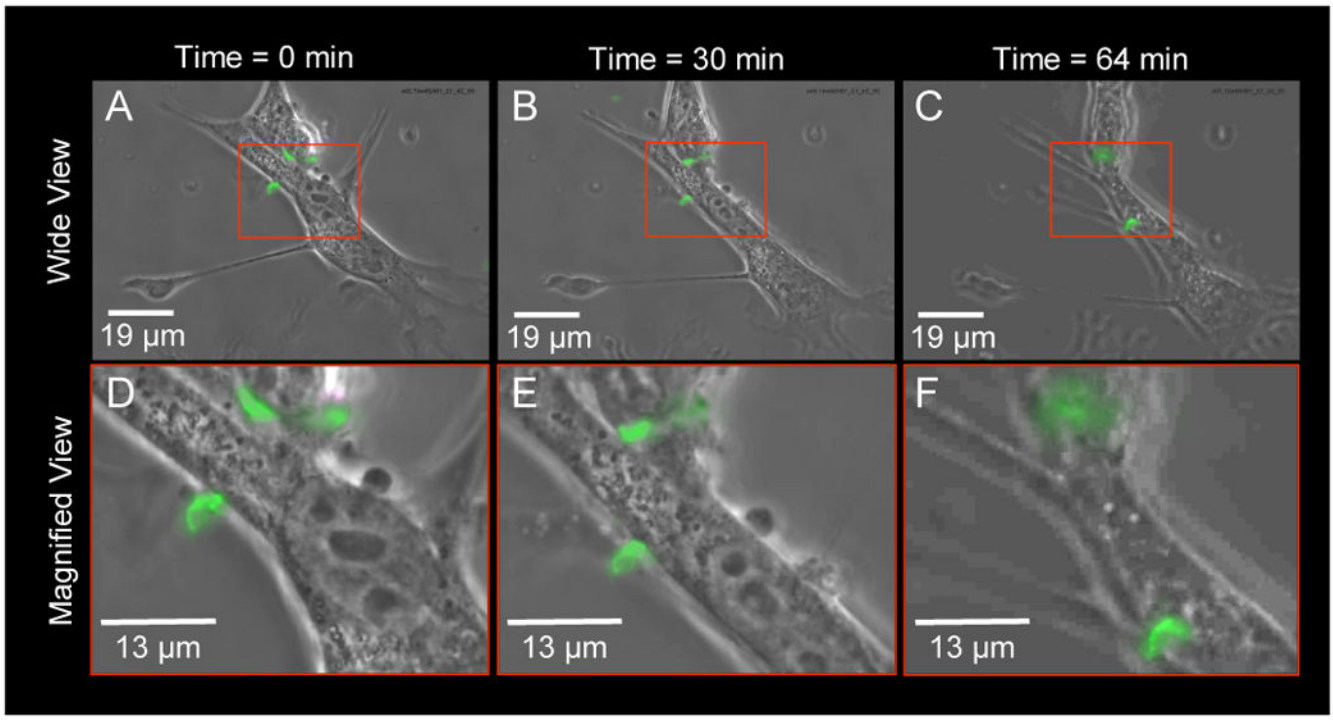


**Figure 7.**

Observation of 3 attached lipid debris particles over time on the surface of two 4T1 murine breast cancer cells at three different time points. The top two particles are on one cell and the bottom particle is on a separate cell. **Panels A, B, and C** show the wide field view of the cell with the green colored lipid particles that were left attached to the cell surface after microbubble destruction with low peak negative pressure ultrasound. **Panels D, E and F** show the magnified view of the lipid debris for each time point. After 64 min of observation the lipid particles were seen to translate over the cell surface as the cell itself moved and changed shape. The right most particle of the two at the top moved 6 µm towards the left. The particle at the bottom translated 21µm. The lipid particles were not seen to change shape or to integrate into the cell surface.

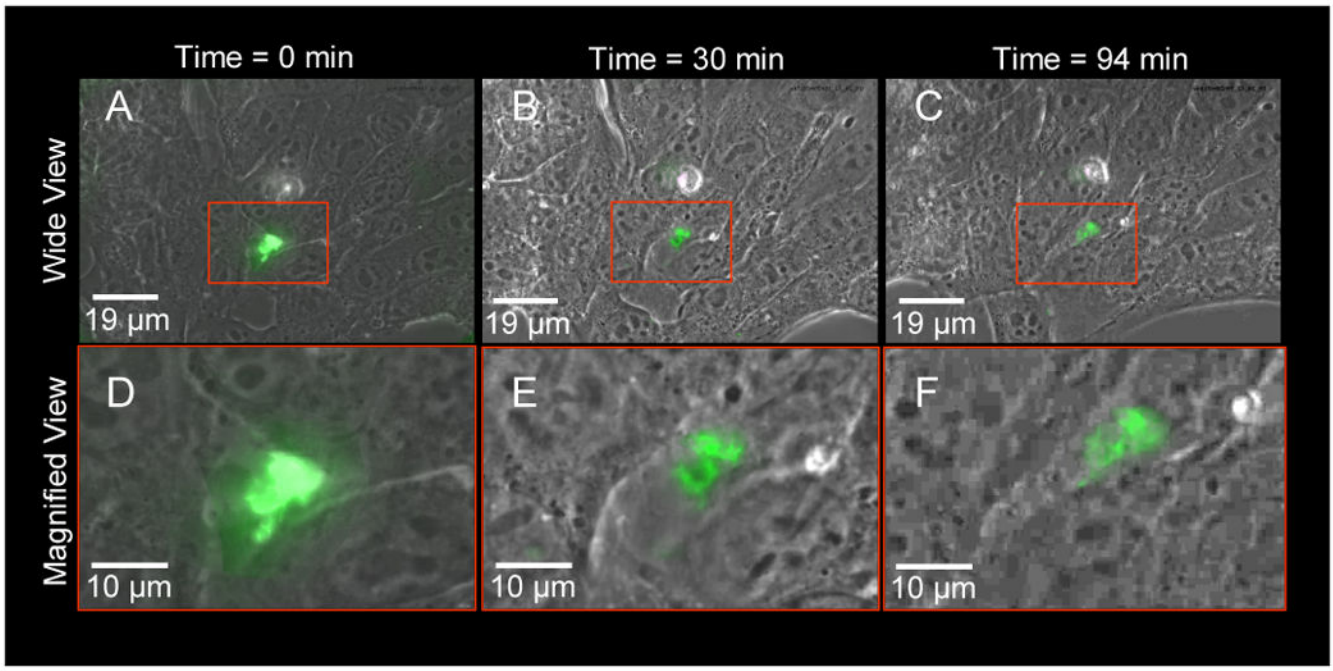


**Figure 8.**

Observation of 1 attached lipid debris particle over time on the surface of a single 4T1 murine breast cancer cell that is part of a confluent group of cells at three different time points. The confluent nature of the cells simulates the conditions of an actual tumor tissue. **Panels A, B, and C** show the wide field view of the confluent cells with the particle in green. **Panels D, E and F** show the magnified view of the particle at the three time points. Here the particle translated by 8μm and rotated 20° clockwise. The rotation and translation was less than that observed with the cells shown in Figures 4 and 5 probably due to the confluency of the cells inhibiting the same degree of motion seen with the single free cells. The particle also appeared to stretch along its long axis but did not appear to integrate into the cell membrane.

**Table 1**

**Summary of observed lipid fragment behavior on the surface of the cells**

| Cell Type | Cell State | N | Number of Attached Microbubbles | Resulting Debris | Ultrasound Peak Negative Pressure in MPa | Time of Observation | Observed Lipid Behavior |
|---|---|---|---|---|---|---|---|
| 4T1 | Single Cell | 2 | 1 | Visible lipid debris particles left at site of microbubble attachment | 0.18 | 9s | Remained on cell surface |
| 4T1 | Single Cell | 1 | 2 | Visible lipid debris particles left at site of microbubble attachment | 0.18 | 9s | Remained on cell surface |
| 4T1 | Single Cell | 2 | >2 | Visible lipid debris particles left at site of microbubble attachment | 0.18 | 9s | Remained on cell surface |
| HUVEC | Single Cell | 1 | 1 | Visible lipid debris particles left at site of microbubble attachment | 0.8 | 8s | Remained on cell surface |
| 4T1 | Small Non-Confluent Group | 1 | 1 | Individual lipid debris particles observed | 0.18 | 96 min | Remained on cell surface. It rotated 90° clockwise and then 130° counter-clockwise and translated 11μm |
| 4T1 | Small Non-Confluent Group | 1 | 1 | Individual lipid debris particles observed | 0.18 | 96 min | Remained on cell surface. The top two particles moved towards each other. The particle at the bottom moved down by 21μm. |
| 4T1 | Confluent Group | 1 | 2 | Individual lipid debris particles observed | 0.18 | 64 min | Remained on cell surface. It rotated 20° clockwise and translated 8μm |